



RESEARCH LETTER

10.1029/2018GL078650

Key Points:

- Numerical models of heterogeneous faults reproduce observations of earthquake clusters with constant duration but variable seismic moment
- The constant duration is controlled by the fault size, while the variable seismic moment depends on the fraction of the fault rupturing
- On-fault stress drops are constant at ~3 MPa, but their seismological estimates increase from 0.006 to 8 MPa due to the source complexity

Supporting Information:

- Supporting Information S1

Correspondence to:

Y.-Y. Lin,
yenyulin@caltech.edu

Citation:

Lin, Y.-Y., & Lapusta, N. (2018). Microseismicity simulated on asperity-like fault patches: On scaling of seismic moment with duration and seismological estimates of stress drops. *Geophysical Research Letters*, 45. <https://doi.org/10.1029/2018GL078650>

Received 10 MAY 2018

Accepted 19 JUL 2018

Accepted article online 25 JUL 2018

Microseismicity Simulated on Asperity-Like Fault Patches: On Scaling of Seismic Moment With Duration and Seismological Estimates of Stress Drops

Yen-Yu Lin¹  and Nadia Lapusta^{1,2} 

¹Seismological Laboratory, California Institute of Technology, Pasadena, CA, USA, ²Mechanical and Civil Engineering, California Institute of Technology, Pasadena, CA, USA

Abstract Observations show that microseismic events from the same location can have similar source durations but different seismic moments, violating the commonly assumed scaling. We use numerical simulations of earthquake sequences to demonstrate that strength variations over seismogenic patches provide an explanation of such behavior, with the event duration controlled by the patch size and event magnitude determined by how much of the patch area is ruptured. We find that stress drops estimated by typical seismological analyses for the simulated sources significantly increase with the event magnitude, ranging from 0.006 to 8 MPa. However, the actual stress drops determined from the on-fault stress changes are magnitude-independent and ~3 MPa. Our findings suggest that fault heterogeneity results in local deviations in the moment-duration scaling and earthquake sources with complex shapes of the ruptured area, for some of which stress drops may be significantly (~100–1,000 times) underestimated by the typical seismological methods.

Plain Language Summary Microseismicity, that is, relatively small earthquake ruptures that occur much more frequently than large, destructive ones, is actively studied to understand properties of seismogenic faults in the Earth's crust. The properties of interest include earthquake durations, sizes, and stress drops that describe how much fault loading an earthquake has relieved. Observations show that microseismic ruptures from the same fault area can have similar source durations but different sizes, violating the commonly assumed scaling between the duration and size. Our numerical simulations of a sequence of ruptures on a fault patch explain such behavior by heterogeneous fault patch properties. We also compare the stress drops for the simulated ruptures obtained directly from our modeling and inferred from the ground motion produced on the surface, as done for natural earthquakes, find significant discrepancies between them, and explain the discrepancies by the complex shapes of the rupture areas of the simulated events.

1. Introduction

Large, destructive earthquakes are rare, particularly in a given locale, and hence one of the main observational windows into the state of the crustal faults that host them and their physics is microseismicity that occurs in the interseismic period between large events. Two important—and related—influential conclusions about seismicity have resulted from the observations of both microseismicity and large events. First, the average static stress drops in earthquakes with magnitudes ranging from 0.0 to 8.5, taken collectively, appear to be magnitude-independent, albeit with a large scattering from 0.1 to 100 MPa (Abercrombie, 1995; Allmann & Shearer, 2009; Goebel et al., 2017; Hauksson, 2015; Hough, 1996; Humphrey & Anderson, 1994; Mori & Frankel, 1990; Shearer et al., 2006). Second, the source duration t_w is proportional to the seismic moment M_0 to the power of 1/3 (Aki, 1967; Duputel et al., 2013; Houston, 2001):

$$t_w \propto M_0^{1/3} \quad (1)$$

The confidence in the conclusions is strengthened by the fact that they are related through a relatively simple earthquake source model of a circular crack expanding axisymmetrically with a constant rupture speed and spatially uniform stress drop, in which the magnitude-independent stress drop indeed corresponds to the moment-duration scaling of (1); we refer to such a source as the traditional source model in the following. This self-consistency is not fully reassuring, however, since the two observations are not independent for microseismicity, in that the stress drops are, in fact, estimated by using methods based on this traditional

model (Abercrombie, 1995; Allmann & Shearer, 2009; Goebel et al., 2015, 2017; Lin et al., 2012; Shearer et al., 2006; Uchide et al., 2014).

More detailed studies of microseismicity ($M_w < 3.0$) reveal that some earthquake clusters may not follow the general scaling relation. For example, a study of small earthquakes in Parkfield, California (Harrington & Brodsky, 2009) found different seismic moments for sources of the same duration. Similar observations were made for repeating earthquakes in the earthquake sequence preceding the 1999 Izmit earthquake in Turkey (Bouchon et al., 2011) and for low-frequency earthquakes beneath southern Vancouver Island in Canada (Bostock et al., 2015). Clusters of several earthquakes with constant source duration but large magnitude variations were discovered using the borehole seismometers in Taiwan (Lin et al., 2016). For the seismic clusters, the shapes of the recorded P and S waves of the events are very similar regardless of the event magnitude, indicating that the source durations are essentially constant for all earthquakes in a cluster, despite the event magnitude ranging from M_w 0.3 to 2.0. This observation directly violates the general relation of (1). Note that if the source duration is interpreted in terms of the seismic source dimension using a constant rupture speed, as commonly done (Boatwright, 1980; Lanza et al., 1999; Madariaga, 1976; Shearer, 2009), then the constant duration would correspond to the same rupture size and would imply decreasing average slips and hence decreasing stress drops for events of decreasing magnitudes. Such implication is contrary to the current understanding of microseismicity and earthquake physics. We note that the unusual observations of microseismicity may be affected by unusual path effects, even for instruments at deep boreholes (e.g., Ide et al., 2003), although some studies have applied multiple analysis methods to ensure that that is not the case (e.g., Lin et al., 2016).

Here we explore the hypothesis that strong variations in shear resistance (or strength) over a fault patch could provide a potential explanation of such behavior, with the event duration controlled by the size of the patch and event magnitude determined by how much of the patch area has been ruptured (Figure 1a). To this end, we numerically simulate earthquake sequences on a rate-and-state fault, with a seismogenic patch governed by steady-state velocity-weakening friction surrounded by a steady-state velocity-strengthening region. The seismogenic patch contains strong variations in shear strength due to variable normal stress. Such variations could result, for example, from slightly nonplanar interfaces being compressed into full contact (Brodsky et al., 2011; Candela et al., 2009; Renard et al., 2006; Sagy et al., 2007).

We find that such models indeed lead to the desired behavior, with seismic events of a range of moment magnitudes having the same duration. Furthermore, the actual stress drops of the simulated events, for example, the stress drops calculated directly from the simulated on-fault stress changes, are magnitude-independent and significantly different from the seismically estimated values.

2. Modeling Earthquake Sequences on a Heterogeneous Rate-and-State Patch

2.1. Rate-and-State Friction

Our fault is governed by a laboratory-based description of the shear resistance called rate-and-state friction (Dieterich, 1979, 1981; Marone, 1998; Rice, 1983; Ruina, 1983; Tullis & Weeks, 1986). Fault models based on the rate-and-state friction have been used to reproduce and study a number of earthquake source phenomena, including earthquake nucleation, postseismic slip, aftershocks, earthquake sequences including repeating earthquakes, and patterns of seismogenic and aseismic slip (Barbot et al., 2012; Ben-Zion & Rice, 1997; Dieterich, 1994; Dieterich, 2007; Helmstetter & Shaw, 2009; Kaneko & Lapusta, 2008; Lapusta et al., 2000; Lapusta & Liu, 2009; Lui & Lapusta, 2016; Rice, 1993).

Following Lapusta and Liu (2009), we use the following rate-and-state formulation:

$$\begin{aligned}\tau &= \sigma \left[f^* + a \ln \left(\frac{V}{V^*} \right) + b \ln \left(\frac{V^* \theta}{L} \right) \right] \\ \dot{\theta} &= 1 - \frac{V\theta}{L},\end{aligned}\tag{2}$$

where τ and σ are shear and effective normal stresses, respectively, V is the slip rate, V^* is the slip rate for the reference friction coefficient f^* , θ is an evolving state variable, L is a characteristic slip distance, and a and b are parameters that quantify the rate-and-state effects. Expressions (2) are regularized for zero and negative slip

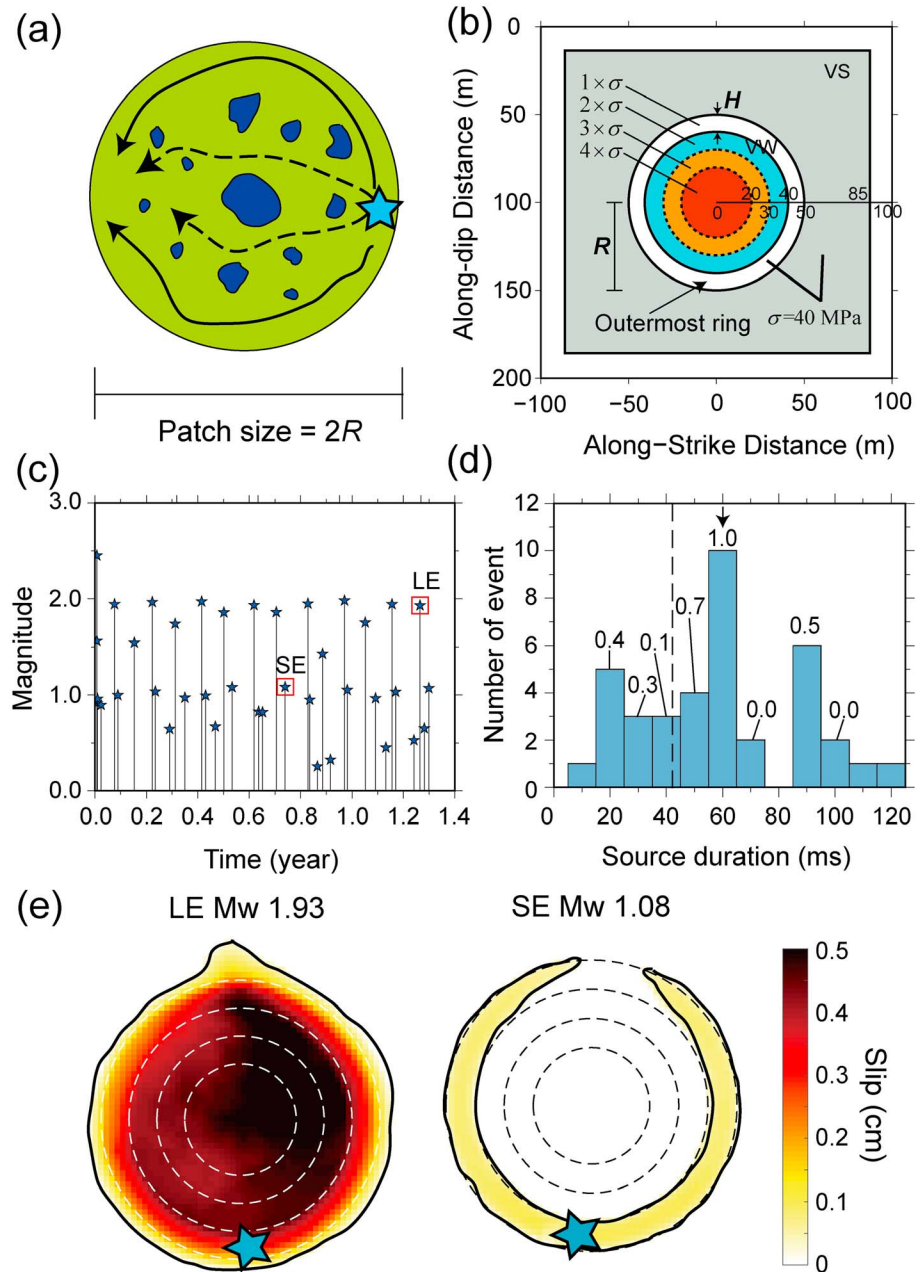


Figure 1. Models that produce events of similar durations but different seismic moments on the same fault patch. (a) A conceptual illustration of a heterogeneous fault patch with several asperities of higher effective normal stress (deep blue regions). The duration of the patch-spanning events would be controlled by the patch size, while their magnitudes would be controlled by how many asperities they rupture. (b) A simplified fault model for our simulations with a single asperity in the center of the velocity-weakening patch of diameter $2R$ surrounded by velocity-strengthening areas (gray). The 2-D fault is embedded into a 3-D elastic medium, and its slip history of earthquake sequences and slow slip is calculated by fully dynamic simulations. (c) The sequence of simulated seismic events, with variable moments. (d) The histogram of the number of events with the source duration binned by 0.01-s increments. The duration of rupture propagation from one side of the patch to the other with the speed of 0.8β is shown by the dashed line. The values above the bars indicate the maximum magnitude difference M_{diff} in the group. (e) Slip distributions for the largest (LE) and smallest (SE) events with the same rupture directivity on the patch (Model III, $H/R = 0.19$). The blue stars indicate the nucleation region of the rupture. The snapshots of the slip rate over the fault for LE and SE are shown in Figure S1. The dashed circles indicate the contours of the normal stress (Figure 1b).

rates (Lapusta & Liu, 2009). The relation for the friction coefficient at steady-state ($V = \text{constant}$, $\theta = L/V$) is given by

$$f_{ss} = f^* + (a - b) \ln\left(\frac{V}{V^*}\right). \quad (3)$$

If $a > b$, then friction increases with the increasing slip rate (velocity strengthening, VS) and, if $a < b$, then friction decreases with the increasing slip rate (velocity weakening, VW). Note that this formulation is simplified and does not fully account for a number of laboratory observations even at slow slip rates (Bhattacharya et al., 2015, 2017). We also do not consider the potential effects of enhanced dynamic weakening (Tullis, 2007, and references therein; Noda & Lapusta, 2010, 2013). Rather, we use this formulation as a convenient tool for simulating sequences of earthquakes with properties similar to observations.

2.2. Model of an Asperity-Like Seismogenic Patch With Variable Normal Stress

We consider a seismogenic circular patch of radius R with steady-state VW friction properties, surrounded by a steady-state VS region. The patch contains a distribution of normal stress with higher values toward the center of the patch, as would arise for a flattened “bump” (often called “asperity”) on the sliding surface (Figure 1b). This is the simplest version of the heterogeneous patch (Figure 1a), with only one peak of the higher normal stress and hence higher friction strength. To promote events of different sizes and simplify the interpretation of the results, the normal stress is increased in steps, from $\sigma = 40$ MPa in the outmost ring to 160 MPa in the center of the patch. At least some events should nucleate at the edges of the patch in this model because the shear stressing is the highest there due to creep in the surrounding VS region and the strength is lowest there due to the smallest σ . But, as slip proceeds, events may also nucleate at other locations of high shear stress.

We make the width H of the outmost ring equal to the nucleation size h^* for the corresponding patch properties, using the following theoretical estimate of h^* appropriate for the values of a and b that we use (Lapusta & Liu, 2009; Rubin & Ampuero, 2005):

$$h^* = \frac{\pi}{2} \frac{\mu}{(1 - \nu)} \frac{bL}{(b - a)^2 \sigma}, \quad (4)$$

where ν is Poisson ratio. We fix the values of all parameters in (4) except for L to the ones commonly used in modeling (e.g., Lapusta & Liu, 2009; Table S1 in the supporting information) and then change h^* and hence H by changing the characteristic slip distance L . To obtain earthquake moments similar to the ones reported in Lin et al. (2016), we choose the patch radius R to be 50 m.

Using the methodology of Lapusta and Liu (2009), we simulate long-term slip in Models I–IV with $H/R = 0.55$, 0.27, 0.19, and 0.14, which correspond to $L = 20$, 10, 7, and 5 μm and $h^* = 27.5$, 13.7, 9.6, and 5 m (Text S1 and Table S2 in the supporting information). For each model, we generate a sequence of 40 seismic events using 500 CPUs and ~ 100 hr of calculation time. The simulation approach used resolves all wave-mediated inertial effects during seismic events.

3. Earthquake Clusters With Events of Similar Duration But Different Magnitudes

Our simulations result in sequences of seismic events with different moment magnitudes, depending on whether the entire patch is ruptured or not, as expected. For example, the long-term simulations of Model III result in earthquakes with significant magnitude variations as shown in Figure 1c. Since we are interested in events maintaining similar source duration, we group events by their source duration (Figure 1d). Although the source durations for all the events vary from less than 0.01 to 0.13 s, many events have similar source durations. The bin with the largest number of events is centered on 0.060 s, the duration slightly larger than the 0.042 s needed for the rupture with the speed of 0.8β to propagate from one side of the patch to the other. The rupture duration in our simulations is defined as the time during which at least one cell on the fault slips faster than 0.1 m/s, consistent with the previous studies (Bizzarri & Belardinelli, 2008; Lapusta & Liu, 2009; Noda & Lapusta, 2013; Rubin & Ampuero, 2005).

We focus on the events in this bin and investigate their magnitude variation and rupture behavior. The largest and smallest events in the group with the same rupture directivity are event 38 (M_w 1.93) and event 24 (M_w 1.08), respectively, which are named LE and SE in the following. The magnitude difference for the events is $M_{\text{diff}} = 0.85$, but their source durations are both ~ 0.06 s (Figure 2a). The LE ruptures the entire VW patch, but the rupture of the SE only propagates on the outermost ring of the patch (Figures 1e and S1 and Table S2 in the supporting information). The rupture areas and average slips for LE and SE are different by factors of 3.6 and 5.8, respectively. The combined differences in slip and area produce a factor of ~ 20 in their seismic moments based on

$$M_0 = \mu A \bar{\delta}, \quad (5)$$

where μ , A , and $\bar{\delta}$ are the shear modulus, rupture area, and average slip, respectively. Their similar source durations, set by the patch size, violate the commonly assumed scaling, $t_w \propto M_0^{1/3}$.

Hence, we successfully produce events on the patch with similar source durations but significant magnitude variations, consistent with the observations of Lin et al. (2016). The maximum magnitude difference from the modeling is in Model IV (with the smallest H/R ratio), from M_w 0.94 to 1.99, with the magnitude difference of $M_{\text{diff}} = 1.05$ (Table S2). This is not fully consistent with the variation of M_w from 0.27 to 1.97 with $M_{\text{diff}} = 1.7$ obtained in the observational study of Lin et al. (2016), but of the same order. To produce events with similar duration but magnitude differences larger than the 1.05 of Model IV, one needs to continue decreasing the ratio H/R , which is expensive computationally. We predict that $H/R = 0.02$ can match $M_{\text{diff}} = 1.7$ (Text S2 and Figure S3).

The far-field seismic waveforms, computed by the procedure described in Text S3, for LE and SE (Figure 2e) confirm the similar durations of about 0.06 s, as in the observations. Their shapes (Figure 2d) are similar but not as similar as in the observations of Lin et al. (2016), suggesting that the smallest events in the observations may have more complex rupture patterns than those of our simulations, perhaps more consistent with the schematics in Figure 1a. The maximum far-field amplitudes for the P wave for LE and SE (Figure 2e) have the ratio of ~ 23 , which is consistent with the observations for events of similar magnitudes (Lin et al., 2016, Figure 7a). From the P wave spectra, we find that the high-frequency fall-off is slower in SE compared to that in LE (Figure 2g), indicating that SE contains more high-frequency signals. This is consistent with the observations (Lin et al., 2016, Figure 9).

4. Large Discrepancy Between Actual and Seismologically Inferred Stress Drops

4.1. Stress Drop From On-Fault Variations in Shear Stress

We calculate the energy-based average stress drop (Noda et al., 2013), which weights the stress drop distribution at the source by the final slip distribution:

$$\Delta\sigma_E = \frac{\int_{\Sigma} \Delta\sigma \cdot \Delta u ds}{\int_{\Sigma} \Delta u ds}, \quad (6)$$

where $\Delta\sigma$ and Δu are the stress drop and final slip, respectively, at each point inside the rupture area Σ .

The energy-based stress drops are ~ 3 MPa for all events (Table S2 and Figure 3a). The energy-based stress drop calculated here is the actual stress drop at the source, since it is computed from the distribution of the stress change over the fault. As mentioned in section 1, the same stress drop for events of the same duration but different magnitudes contradicts the common interpretation, in which the same duration would correspond to the same source area (not true in our simulations) and then the different magnitudes would be interpreted as a difference in average slip and hence stress drops.

4.2. Stress Drop From Seismic Signals

We calculate the seismically estimated stress drop for the events through the commonly used seismological methods based on the spectral analysis. We (i) assume that the simulated earthquake sources are located on a pure strike-slip fault with a vertical fault plane and the source focal depth of 10 km; (ii) put 16 pseudo stations on the surface in a 60×60 km² region with an equal spatial interval of 20 km, producing a broad station

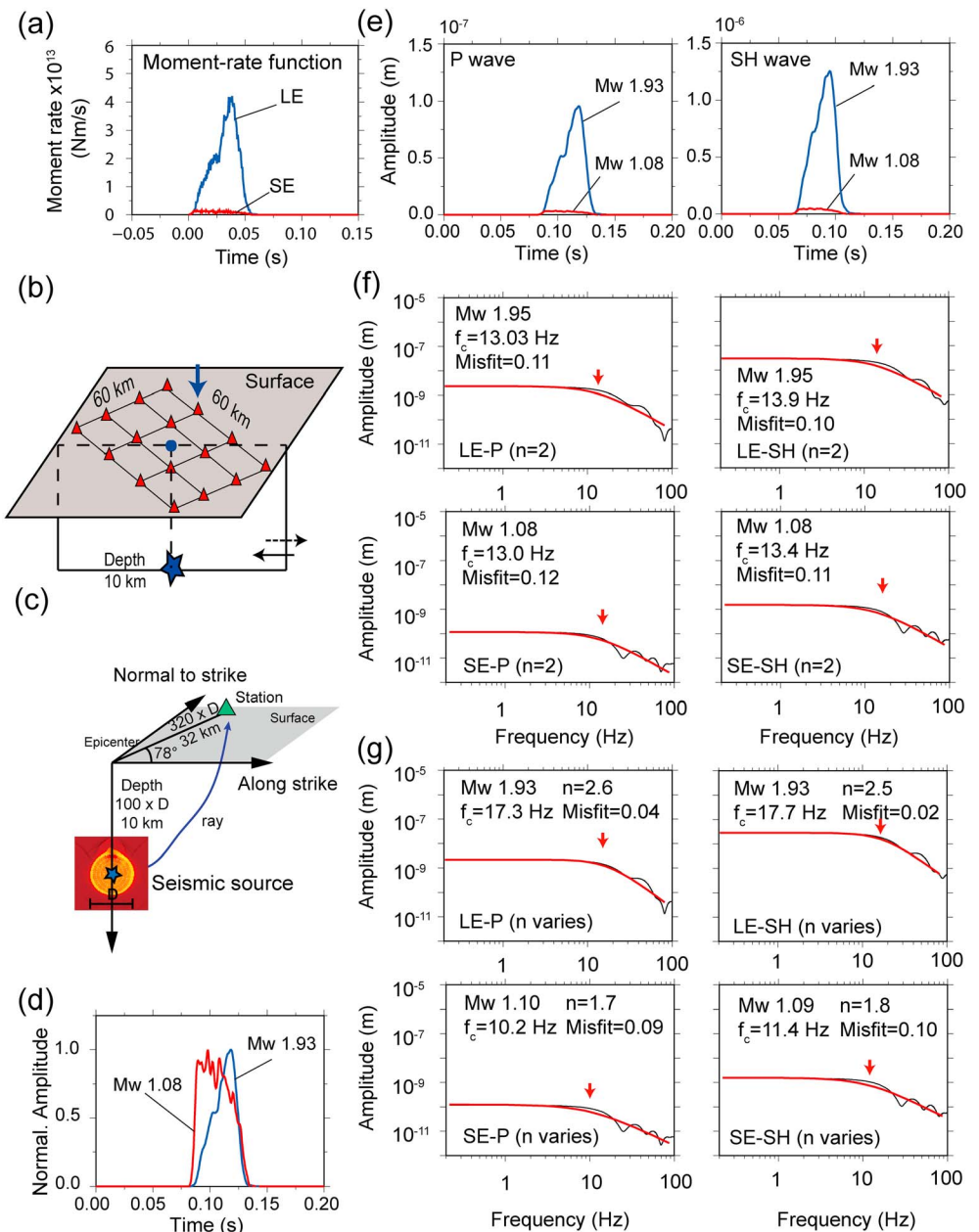


Figure 2. Synthetic waveforms for the events largest event (LE, M_w 1.93) and smallest event (SE, M_w 1.08) from Figure 1e. (a) Moment-rate functions for the two events with much different amplitudes but similar source durations. (b) The geometry of the seismic source and 16 pseudo stations on the surface. Note that the vertical dimension is exaggerated in this illustration; the more dimensionally accurate illustration is given in Figure S4. The blue arrow indicates the location of the station for (c)–(g). (c) The source-station geometry of the station for showing the synthetic waveforms. The assumed epicenter distance of 32 km is 320 times larger than the source diameter D , indicating a far-field station. (d) Comparison of normalized P wave synthetics between the LE and SE events processed with a low-pass filter of 200 Hz. (e) The synthetics of the P and SH waves for the LE and SE events with their actual amplitudes. (f) The P and SH spectra for the two events (black) and the best fits based on the theoretical source spectrum (red) with the source model of $n = 2$. The source parameters calculated from the spectral fitting analysis based on the work of Madariaga (1976) are shown as inserts. (g) The P and SH spectra for the two events (black) and the best fits based on the theoretical source spectrum (red) with the source model of adjustable n .

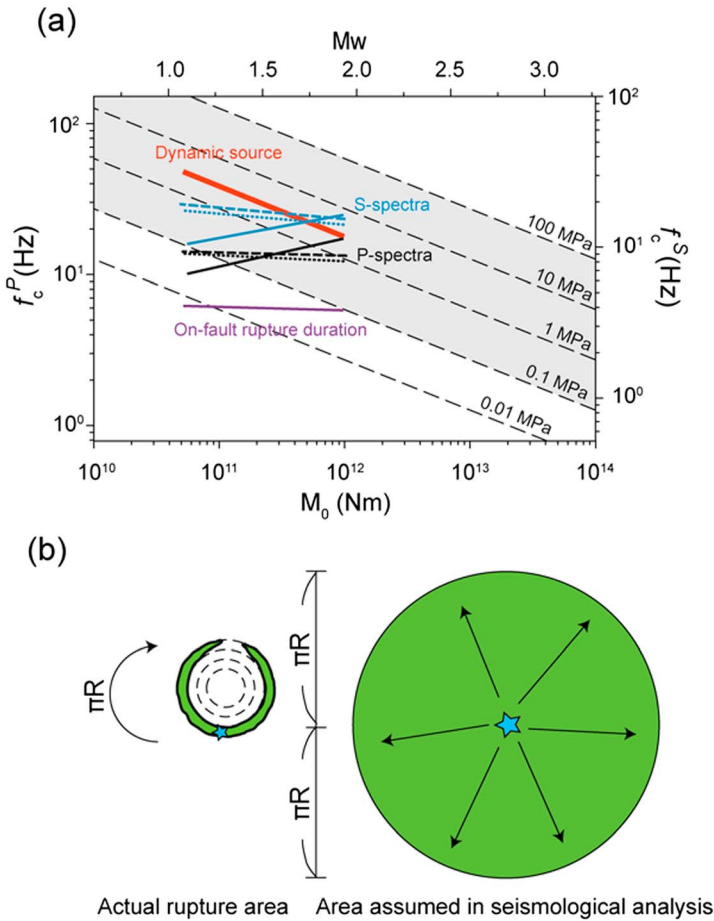


Figure 3. (a) Comparison, for Model III, of the stress drop estimates from the dynamic source models directly (red line) and their synthetic seismograms (the black, blue, and purple lines for the source dimension estimated from the P spectrum, S spectrum, or on-fault rupture duration, respectively; the dashed and solid lines for the spectral fits of $n = 2$ and adjustable n , respectively; dotted lines for the P and S spectra with $n = 2$ and pseudo stations on the entire focal sphere). The actual energy-averaged stress drops are nearly constant for the two events and ~ 3 MPa, while the seismological estimates span a range from 0.006 to 8 MPa. The gray region demonstrates the general range for stress drop estimates of natural earthquakes (Allmann & Shearer, 2009). Note the different vertical scales for the corner frequencies based on the P wave and S wave spectrum. (b, left) The large discrepancy between the actual and seismically estimated stress drops is mainly due to the large difference between the actual rupture area (e.g., smallest event) and (right) the area computed based on the event duration in the theoretical models used to estimate stress drops from seismograms.

coverage (Figures 2b and S4); (iii) simulate synthetic far-field waveforms on these stations for both P and SH waves of all events, following the procedure described in Text S3; (iv) find the estimated duration of the source from the corner frequency in the spectral domain (Text S4); (v) estimate the source radius R from these durations using a constant rupture speed; and (vi) calculate the seismically estimated stress drop $\Delta\sigma$ by the commonly used relation (Eshelby, 1957; Madariaga, 1976):

$$\Delta\sigma = \frac{7M_0}{16r^3} = \frac{7\pi^{3/2}}{16} \frac{M_0}{A^{3/2}} \quad (7)$$

We also compute the seismological stress drop estimates that would result from applying commonly used steps (v)–(vi) to the exact knowledge of the on-fault source duration. In addition to the spectral methods considered in this work, the source duration can be estimated by other means, for example, from time domain approaches, typically based on the width of the far-field P wave displacement pulse or combination of that with the spectral methods (e.g., Boatwright, 1980; Lanza et al., 1999; Lin et al., 2016).

We determine the corner frequency f_c for the P and SH waves by applying the spectral fitting method. The approach is the current state-of-art technique for estimating source parameters of observable small earthquakes (Abercrombie, 1995; Allmann & Shearer, 2009; Goebel et al., 2015, 2017; Lin et al., 2012; Shearer et al., 2006; Uchide et al., 2014) as well as for investigating characteristics of seismic signals from simulated source models (Kaneko & Shearer, 2014, 2015; Madariaga, 1976; Sato & Hirasawa, 1973; Wang & Day, 2017). The spectrum of the displacement amplitude is fit by

$$A(f) = \frac{\Omega_0}{[1 + (f/f_c)^n]}, \quad (8)$$

where Ω_0 is the amplitude level at low frequencies related to the seismic moment M_0 , f_c is the corner frequency which is inversely proportional to the duration of source time function, and n is the high-frequency fall-off rate of the spectrum (Shearer, 2009). The approach with $n = 2$ is often called the omega-square model (Aki, 1967; Boatwright, 1980; Brune, 1970). Some source models and observations indicate different fall-off rates at high frequencies (e.g., Dahlen, 1974; Uchide & Imanishi, 2016). Here we consider two types of the fit, one with $n = 2$ and the other with adjustable n that provides the best fit to the spectrum. The fitting procedure is described in Text S4. After averaging the estimated f_c from all stations, we calculate the source dimension R using (Madariaga, 1976):

$$R = \frac{C\beta}{f_c}, \quad (9)$$

where C is 0.32 and 0.21 for the P and S spectra, respectively. Note that the values of C depend on the assumed rupture speed, and these commonly used values correspond to the rupture speed of 0.9β , a typical value for the analysis of natural events as well as a value close to the average rupture speed for our events. The obtained source dimension is the product of the source duration and the assumed rupture speed of 0.9β and implies the source duration of

$$t_w = \frac{R}{0.9\beta} = \frac{C}{0.9f_c}. \quad (10)$$

Note that this spectral analysis has been developed, assuming the traditional source model of a circular crack expanding axisymmetrically with a constant rupture speed and spatially uniform stress drop. We have tested

our implementation of the spectral analyses using simpler dynamic sources that start in the center of the patch and spread with near-constant rupture speeds, similar to the work of Kaneko and Shearer (2015), and obtained results for durations and stress drops similar between the simulations and spectral analyses, in line with the comparison in Kaneko and Shearer (2015).

The fitting results for one of the pseudo stations (Figures 2b and 2c) in the spectral domain are shown in Figures 2f and 2g. Both $n = 2$ and the adjustable n approaches fit the synthetic spectra well, but the adjustable n approach results in a smaller misfit. This improvement suggests that the fall-off rate n may vary for different events. The SE has $n = 1.8$, smaller than 2, and the LE has $n = 2.5$, larger than 2. This difference in the fall-off rate n reflects differences in the rupture behavior between the two events, which would be important to systematically investigate for different types of earthquake sources.

The seismologically inferred estimates of the average stress drop systematically increase for larger events for all approaches and models we considered (Table S3), as expected and illustrated in Figure 3a for Model III. For example, with the source-spectrum model of $n = 2$, the estimated stress drops are 0.07 and 1.21 MPa from the P wave and 0.60 and 6.45 MPa from the S wave spectra for the SE and LE, respectively. Furthermore, we find a significant (factor of 5 to 9) difference between the stress drops estimates based on the P wave versus S wave spectra, which is due to the different ratio of P to S wave corner frequency in our simulated sources (Table S3), of about ~ 1 , than that of about 1.5 for the traditional source model as analyzed by Madariaga (1976). The discrepancy of stress drop estimates between different approaches is further discussed in the Text S5.

Note that we use a network of surface stations for the seismological estimates to mimic the approach typically taken in the observational studies (Abercrombie, 1995; Allmann & Shearer, 2009; Goebel et al., 2015, 2017; Lin et al., 2012; Shearer et al., 2006; Uchide et al., 2014). We have verified that the results remain qualitatively and quantitatively similar for the analysis based on the entire focal sphere, which can be done in this synthetic study but cannot be used in practice; for example, the results for the spectral analysis with $n = 2$ based on the pseudo stations on the entire focal sphere are shown in Figure 3a as dotted lines.

4.3. Comparison of the Actual and Seismologically Inferred Stress Drops

The actual average static stress drops from the simulated sources are approximately the same for all simulated events, ~ 3 MPa (section 4.1), while the seismologically inferred stress drops (section 4.2) increase from 0.006 to 8 MPa as the seismic moment increases (Figure 3a). The largest difference between the actual and seismologically inferred stress drops, by a factor of up to 100–1,000, occurs for the smallest ring-like earthquake sources (Table S4). The work of Kaneko and Shearer (2015) demonstrated that a factor of ~ 10 in stress drop discrepancy can result simply from unidirectional versus axisymmetric propagation and the associated difference in rupture area.

Here we find that a completely different shape of the ruptured area than the typically assumed circle can be a natural outcome of a reasonable fault model and can result in an even larger discrepancy. Our smallest ring-like events have significantly smaller rupture area compared to the traditional, spreading-from-the-center, circular source models of the same duration (Figure 3b, Table S4, and Text S5). Once we apply the seismological analyses from section 4.2, we replace the ring-like sources with the traditional circular sources of much larger area, overestimating the source area and hence underestimating the stress drop by large factors (of ~ 30 and ~ 500 , respectively, in the case of the analysis based on the actual event duration for Model III illustrated in Figure 3b). The directivity effect pointed out by Kaneko and Shearer (2015) contributes to this discrepancy in the rupture area, since our sources do not spread axisymmetrically but rather propagate from one side of the ring to the other. For the events considered here, the discrepancy between the actual source area and the one assumed in the typical seismological analyses is the largest when the exact event duration is assumed to be known, since the spectral methods systematically underestimate the duration (by factors ranging from 0.21 to 0.76 for the smallest ring-like events, Table S4 and Text S5), reducing the seismologically estimated rupture area and hence partially compensating for the incorrect assumption of the rupture shape.

To further illustrate the dominating effect of the incorrect estimate of the rupture area on the estimates of stress drops, let us estimate the stress drops using the traditional formula (7) but using the (correct) rupture area from the simulations. For the smallest, ring-like events, these correct-area estimates of the stress drops, which we denote $\Delta\sigma_{M_r}^*$, match the actual stress drops within a factor of 4 (Table S2), rather than the factors of

100–1,000 discussed before. The remaining discrepancy in stress drops is likely due to two factors: (i) Formula (7) rigorously holds for a circular rupture of a uniform stress drop and would be inaccurate for the ruptures of varying stress drops and/or other area shapes, and (ii) the moment-based stress drop estimate $\Delta\sigma_M^*$ and the energy-based stress drops $\Delta\sigma_E$ represent different averages of the stress change field and hence result in somewhat different estimates (Noda et al., 2013).

5. Conclusions

Our modeling shows that the observations of earthquake clusters with similar durations but different seismic moments can be explained by slip patterns on a seismogenic patch with heterogeneous strength. For a subset of events occurring on such a patch, the near-constant duration is set by the patch size, while the seismic moment depends on the fraction of the area ruptured in the event. Smaller rupture areas result in smaller slips, further amplifying the variation in seismic moment.

We have demonstrated this behavior in a highly simplified model of a patch with the effective normal stress increasing toward the center of the patch, as would conceptually occur for a single flattened “bump” on the fault interface. The SEs occur as ring-like sources around the patch perimeter, with the width of the ring being comparable to the nucleation size on the patch, while the LEs rupture the entire patch. We have adjusted our model to produce events with the source duration and magnitudes that explain some of the observations from Lin et al. (2016). The difference in magnitudes that we are able to produce is smaller than in the observations, but our results suggest that simulations with even smaller nucleation sizes would result in larger magnitude variations.

The synthetic far-field seismic signals obtained based on our sources are broadly consistent with the target observations. However, the shapes of the waveforms for the events of different magnitudes are not as similar as in observations. This may indicate that the actual sources are more complex, resulting on patches with a more varied pattern of heterogeneity, as in the conceptual drawing of Figure 1a.

These findings suggest that local event clusters may indeed deviate from the standard scaling relation between the seismic moment and event duration, and such deviation can potentially point to heterogeneous source properties.

Importantly, the actual average stress drops computed in our model and their seismological estimates based on the traditional spectral analysis significantly differ. The actual stress drops, even for the events of different moment but the same duration, are nearly the same, around 3 MPa. At the same time, the seismologically inferred stress drops increase from 0.006 to 8 MPa as the event moment increases. The largest discrepancy between the actual and estimated stress drops, by factors as large as ~ 100 –1,000, results for the smallest analyzed events which are ring-like.

Our stress drop results reveal that the standard seismological analyses may systematically underestimate stress drops for small events with more complex rupture shapes, which could be quite common on heterogeneous faults (Chen et al., 2016; Dreger et al., 2007; Wald & Heaton, 1994). Any small event occurring along a stretch of stress concentration or lower friction resistance would have the shape of that feature. That shape is ring-like in our model but may have other geometry, for example, following the (potentially curved) boundary of the stress concentration of the previously arrested larger event or of the creeping-locked transition, or following a patchwork of favorable stress due to complex prior slip or heterogeneous strength, as in our model. The microseismic sources are indeed observed to be irregular and complex (Chen et al., 2016; Dreger et al., 2007), unlike the traditional circular source models with uniform stress drops and elliptical slip profiles codified in the standard seismological methods (e.g., Madariaga, 1976; Sato & Hirasawa, 1973). For such more complex sources, the rupture area would not be directly related to the source duration and could in fact be much smaller, as illustrated by our simulations.

To capture these important deviations between the standard source models and potentially different microseismicity sources, more detailed seismological analysis would be needed. For example, the recent method for estimating source parameters based on second moments (McGuire, 2017; McGuire & Kaneko, 2018), which provides better estimates for rupture areas, may work much better for our sources. More detailed spectral analyses may also help; for example, the simulated events have a significantly different ratio of the *P* wave to *S* wave corner frequencies in comparison to the one for the Madariaga source model. More

work is needed to evaluate whether such differences can be systematically exploited for better characterization of the microseismicity sources.

Acknowledgments

This study was supported by the National Science Foundation (grants EAR-1520907 and 1724686), United States Geological Survey (grant G16AP00117), Southern California Earthquake Center (SCEC, funded by NSF Cooperative Agreement EAR1033462 and USGS Cooperative Agreement G12AC20038), and the Postdoctoral Research Abroad Program 105-2917-I-564-015 of the Ministry of Science and Technology in Taiwan. This is SCEC contribution 8066. We thank Emily E. Brodsky, Egill Hauksson, Junle Jiang, Hiroo Kanamori, Yoshihiro Kaneko, Valère R. Lambert, Zachary E. Ross, and Natalie Schaal for helpful discussions. We also thank the Associate Editor and two anonymous reviewers for insightful comments that helped us improve the manuscript. The data used are listed in the references, tables, and supporting information.

References

Abercrombie, R. E. (1995). Earthquake source scaling relationships from -1 to 5 ML using seismograms recorded at 2.5-km depth. *Journal of Geophysical Research*, *100*(B12), 24015–24036. <https://doi.org/10.1029/95JB02397>

Aki, K. (1967). Scaling law of seismic spectrum. *Journal of Geophysical Research*, *72*(4), 1217–1231. <https://doi.org/10.1029/JZ072i004p01217>

Aki, K., & Richards, P. G. (2002). *Quantitative seismology*. Sausalito, CA: University Science Books.

Allmann, B. P., & Shearer, P. M. (2009). Global variations of stress drop for moderate to large earthquakes. *Journal of Geophysical Research*, *114*, B01310. <https://doi.org/10.1029/2008JB005821>

Barbot, S., Lapusta, N., & Avouac, J. P. (2012). Under the hood of the earthquake machine: Toward predictive modeling of the seismic cycle. *Science*, *336*(6082), 707–710. <https://doi.org/10.1126/science.1218796>

Ben-Zion, Y., & Rice, J. R. (1997). Dynamic simulations of slip on a smooth fault in an elastic solid. *Journal of Geophysical Research*, *102*(B8), 17,771–17,784. <https://doi.org/10.1029/97JB01341>

Bhattacharya, P., Rubin, A. M., Bayart, E., Savage, H. M., & Marone, C. (2015). Critical evaluation of state evolution laws in rate and state friction: Fitting large velocity steps in simulated fault gouge with time-, slip-, and stress-dependent constitutive laws. *Journal of Geophysical Research: Solid Earth*, *120*, 6365–6385. <https://doi.org/10.1002/2015JB012437>

Bhattacharya, P., Rubin, A. M., & Beeler, N. M. (2017). Does fault strengthening in laboratory rock friction experiments really depend primarily upon time and not slip? *Journal of Geophysical Research: Solid Earth*, *122*, 6389–6430. <https://doi.org/10.1002/2017JB013936>

Bizzarri, A., & Belardinelli, M. E. (2008). Modelling instantaneous dynamic triggering in a 3-D fault system: Application to the 2000 June South Iceland seismic sequence. *Geophysical Journal International*, *173*(3), 906–921. <https://doi.org/10.1111/j.1365-246X.2008.03765.x>

Boatwright, J. (1980). A spectral theory for circular seismic sources; simple estimates of source dimension, dynamic stress drop, and radiated seismic energy. *Bulletin of the Seismological Society of America*, *70*(1), 1–27.

Bostock, M. G., Thomas, A. M., Savard, G., Chuang, L., & Rubin, A. M. (2015). Magnitudes and moment-duration scaling of low-frequency earthquakes beneath southern Vancouver Island. *Journal of Geophysical Research: Solid Earth*, *120*, 6329–6350. <https://doi.org/10.1002/2015JB012195>

Bouchon, M., Karabulut, H., Aktar, M., Özalaybey, S., Schmittbuhl, J., & Bouin, M. P. (2011). Extended nucleation of the 1999 Mw 7.6 Izmit earthquake. *Science*, *331*(6019), 877–880. <https://doi.org/10.1126/science.1197341>

Brodsky, E. E., Gilchrist, J. J., Sagy, A., & Colletini, C. (2011). Faults smooth gradually as a function of slip. *Earth and Planetary Science Letters*, *302*(1–2), 185–193. <https://doi.org/10.1016/j.epsl.2010.12.010>

Brune, J. N. (1970). Tectonic stress and the spectra of seismic shear waves from earthquakes. *Journal of Geophysical Research*, *75*(26), 4997–5009. <https://doi.org/10.1029/JB075i026p04997>

Candela, T., Renard, F., Bouchon, M., Brouste, A., Marsan, D., Schmittbuhl, J., & Voisin, C. (2009). Characterization of fault roughness at various scales: Implications of three-dimensional high resolution topography measurements. In Y. Ben-Zion & C. Sammis (Eds.), *Mechanics, structure and evolution of fault zones* (pp. 1817–1851). Basel: Birkhäuser.

Chen, K. H., Chen, I., & Kim, A. (2016). Can slip heterogeneity be linked to earthquake recurrence? *Geophysical Research Letters*, *43*, 6916–6923. <https://doi.org/10.1002/2016GL069516>

Dahlen, F. A. (1974). On the ratio of P-wave to S-wave corner frequencies for shallow earthquake sources. *Bulletin of the Seismological Society of America*, *64*(4), 1159–1180.

Dieterich, J. (1994). A constitutive law for rate of earthquake production and its application to earthquake clustering. *Journal of Geophysical Research*, *99*(B2), 2601–2618. <https://doi.org/10.1029/93JB02581>

Dieterich, J. H. (1979). Modeling of rock friction: 1. Experimental results and constitutive equations. *Journal of Geophysical Research*, *84*(B5), 2161–2168. <https://doi.org/10.1029/JB084iB05p02161>

Dieterich, J. H. (1981). Constitutive properties of faults with simulated gouge. In N. L. Carter, M. Friedman, J. M. Logan, & D. W. Stearns (Eds.), *Mechanical behavior of crustal rocks: the Handin volume* (pp. 103–120). Washington, DC: American Geophysical Union. <https://doi.org/10.1029/GM024p0103>

Dieterich, J. H. (2007). Applications of rate-and state-dependent friction to models of fault slip and earthquake occurrence. In G. Schubert (Ed.), *Treatise on geophysics, volume 4: Earthquake seismology* (pp. 107–129). Amsterdam: Elsevier. <https://doi.org/10.1016/B978-044452748-6/00065-1>

Dreger, D., Nadeau, R. M., & Chung, A. (2007). Repeating earthquake finite source models: Strong asperities revealed on the San Andreas Fault. *Geophysical Research Letters*, *34*, L23302. <https://doi.org/10.1029/2007GL031353>

Duputel, Z., Tsai, V. C., Rivera, L., & Kanamori, H. (2013). Using centroid time-delays to characterize source durations and identify earthquakes with unique characteristics. *Earth and Planetary Science Letters*, *374*, 92–100. <https://doi.org/10.1016/j.epsl.2013.05.024>

Eshelby, J. D. (1957). The determination of the elastic field of an ellipsoidal inclusion, and related problems. *Proceedings of the Royal Society of London, Series A*, *241*(1226), 376–396. <https://doi.org/10.1098/rspa.1957.0133>

Goebel, T. H. W., Hauksson, E., Plesch, A., & Shaw, J. H. (2017). Detecting significant stress drop variations in large micro-earthquake datasets: A comparison between a convergent step-over in the San Andreas Fault and the Ventura thrust fault system, Southern California. *Pure and Applied Geophysics*, *174*(6), 2311–2330. <https://doi.org/10.1007/s00024-016-1326-8>

Goebel, T. H. W., Hauksson, E., Shearer, P. M., & Ampuero, J. P. (2015). Stress-drop heterogeneity within tectonically complex regions: A case study of San Geronio Pass, southern California. *Geophysical Journal International*, *202*(1), 514–528. <https://doi.org/10.1093/gji/ggv160>

Harrington, R. M., & Brodsky, E. E. (2009). Source duration scales with magnitude differently for earthquakes on the San Andreas Fault and on secondary faults in Parkfield, California. *Bulletin of the Seismological Society of America*, *99*(4), 2323–2334. <https://doi.org/10.1785/0120080216>

Hauksson, E. (2015). Average stress drops of Southern California earthquakes in the context of crustal geophysics: Implications for fault zone healing. *Pure and Applied Geophysics*, *172*(5), 1359–1370. <https://doi.org/10.1007/s00024-014-0934-4>

Helmstetter, A., & Shaw, B. E. (2009). Afterslip and aftershocks in the rate-and-state friction law. *Journal of Geophysical Research*, *114*, B01308. <https://doi.org/10.1029/2007JB005077>

Hough, S. E. (1996). Observational constraints on earthquake source scaling: Understanding the limits in resolution. *Tectonophysics*, *261*(1–3), 83–95. [https://doi.org/10.1016/0040-1951\(96\)00058-3](https://doi.org/10.1016/0040-1951(96)00058-3)

Houston, H. (2001). Influence of depth, focal mechanism, and tectonic setting on the shape and duration of earthquake source time functions. *Journal of Geophysical Research*, *106*(B6), 11,137–11,150. <https://doi.org/10.1029/2000JB900468>

- Humphrey, J. R. Jr., & Anderson, J. G. (1994). Seismic source parameters from the Guerrero subduction zone. *Bulletin of the Seismological Society of America*, 84(6), 1754–1769.
- Ide, S., Beroza, G. C., Prejean, S. G., & Ellsworth, W. L. (2003). Apparent break in earthquake scaling due to path and site effects on deep borehole recordings. *Journal of Geophysical Research*, 108(B5), 2271. <https://doi.org/10.1029/2001JB001617>
- Kaneko, Y., & Lapusta, N. (2008). Variability of earthquake nucleation in continuum models of rate-and-state faults and implications for aftershock rates. *Journal of Geophysical Research*, 113, B12312. <https://doi.org/10.1029/2007JB005154>
- Kaneko, Y., & Shearer, P. M. (2014). Seismic source spectra and estimated stress drop derived from cohesive-zone models of circular subshear rupture. *Geophysical Journal International*, 197(2), 1002–1015. <https://doi.org/10.1093/gji/ggu030>
- Kaneko, Y., & Shearer, P. M. (2015). Variability of seismic source spectra, estimated stress drop, and radiated energy, derived from cohesive-zone models of symmetrical and asymmetrical circular and elliptical ruptures. *Journal of Geophysical Research: Solid Earth*, 120, 1053–1079. <https://doi.org/10.1002/2014JB011642>
- Lanza, V., Spallarossa, D., Cattaneo, M., Bindj, D., & Augliera, P. (1999). Source parameters of small events using constrained deconvolution with empirical Green's functions. *Geophysical Journal International*, 137(3), 651–662. <https://doi.org/10.1046/j.1365-246x.1999.00809.x>
- Lapusta, N., & Liu, Y. (2009). Three-dimensional boundary integral modeling of spontaneous earthquake sequences and aseismic slip. *Journal of Geophysical Research*, 114, B09303. <https://doi.org/10.1029/2008JB005934>
- Lapusta, N., Rice, J. R., Ben-Zion, Y., & Zheng, G. (2000). Elastodynamic analysis for slow tectonic loading with spontaneous rupture episodes on faults with rate-and state-dependent friction. *Journal of Geophysical Research*, 105(B10), 23,765–23,789. <https://doi.org/10.1029/2000JB900250>
- Lin, Y. Y., Ma, K. F., Kanamori, H., Song, T. R. A., Lapusta, N., & Tsai, V. C. (2016). Evidence for non-self-similarity of microearthquakes recorded at a Taiwan borehole seismometer array. *Geophysical Journal International*, 206(2), 757–773. <https://doi.org/10.1093/gji/ggw172>
- Lin, Y. Y., Ma, K. F., & Oye, V. (2012). Observation and scaling of microearthquakes from the Taiwan Chelungpu-fault borehole seismometers. *Geophysical Journal International*, 190(1), 665–676. <https://doi.org/10.1111/j.1365-246X.2012.05513.x>
- Lui, S. K., & Lapusta, N. (2016). Repeating microearthquake sequences interact predominantly through postseismic slip. *Nature Communications*, 7, 13020. <https://doi.org/10.1038/ncomms13020>
- Madariaga, R. (1976). Dynamics of an expanding circular fault. *Bulletin of the Seismological Society of America*, 66(3), 639–666.
- Marone, C. (1998). Laboratory-derived friction laws and their application to seismic faulting. *Annual Review of Earth and Planetary Sciences*, 26(1), 643–696. <https://doi.org/10.1146/annurev.earth.26.1.643>
- Marquardt, D. W. (1963). An algorithm for least-squares estimation of nonlinear parameters. *Journal of the Society for Industrial and Applied Mathematics*, 11(2), 431–441. <https://doi.org/10.1137/0111030>
- McGuire, J. J. (2017). A matlab toolbox for estimating the second moments of earthquake ruptures. *Seismological Research Letters*, 88(2A), 371–378. <https://doi.org/10.1785/0220160170>
- McGuire, J. J., & Kaneko, Y. (2018). Directly estimating earthquake rupture area using second moments to reduce the uncertainty in stress drop. *Geophysical Journal International*, 214(3), 2224–2235. <https://doi.org/10.1093/gji/ggy201>
- Mori, J., & Frankel, A. (1990). Source parameters for small events associated with the 1986 North Palm Springs, California, earthquake determined using empirical green functions. *Bulletin of the Seismological Society of America*, 80(2), 278–295.
- Noda, H., & Lapusta, N. (2010). Three-dimensional earthquake sequence simulations with evolving temperature and pore pressure due to shear heating: Effect of heterogeneous hydraulic diffusivity. *Journal of Geophysical Research*, 115, B12314. <https://doi.org/10.1029/2010JB007780>
- Noda, H., & Lapusta, N. (2013). Stable creeping fault segments can become destructive as a result of dynamic weakening. *Nature*, 493(7433), 518–521. <https://doi.org/10.1038/nature11703>
- Noda, H., Lapusta, N., & Kanamori, H. (2013). Comparison of average stress drop measures for ruptures with heterogeneous stress change and implications for earthquake physics. *Geophysical Journal International*, 193(3), 1691–1712. <https://doi.org/10.1093/gji/ggt074>
- Renard, F., Voisin, C., Marsan, D., & Schmittbuhl, J. (2006). High resolution 3D laser scanner measurements of a strike-slip fault quantify its morphological anisotropy at all scales. *Geophysical Research Letters*, 33, L04305. <https://doi.org/10.1029/2005GL025038>
- Rice, J. R. (1983). Constitutive relations for fault slip and earthquake instabilities. In L. Knopoff, V. I. Keilis-Borok, & G. Puzzi (Eds.), *Instabilities in continuous media* (pp. 443–475). Basel: Birkhäuser. https://doi.org/10.1007/978-3-0348-6608-8_7
- Rice, J. R. (1993). Spatio-temporal complexity of slip on a fault. *Journal of Geophysical Research*, 98(B6), 9885–9907. <https://doi.org/10.1029/93JB00191>
- Rubin, A. M., & Ampuero, J. P. (2005). Earthquake nucleation on (aging) rate and state faults. *Journal of Geophysical Research*, 110, B11312. <https://doi.org/10.1029/2005JB003686>
- Ruina, A. (1983). Slip instability and state variable friction laws. *Journal of Geophysical Research*, 88(B12), 10,359–10,370. <https://doi.org/10.1029/JB088iB12p10359>
- Sagy, A., Brodsky, E. E., & Axen, G. J. (2007). Evolution of fault-surface roughness with slip. *Geology*, 35(3), 283–286. <https://doi.org/10.1130/G23235A.1>
- Sato, T., & Hirasawa, T. (1973). Body wave spectra from propagating shear cracks. *Journal of Physics of the Earth*, 21(4), 415–431. <https://doi.org/10.4294/jpe1952.21.415>
- Shearer, P. M. (2009). *Introduction to seismology*. Cambridge University Press. <https://doi.org/10.1017/CBO9780511841552>
- Shearer, P. M., Prieto, G. A., & Hauksson, E. (2006). Comprehensive analysis of earthquake source spectra in southern California. *Journal of Geophysical Research*, 111, B06303. <https://doi.org/10.1029/2005JB003979>
- Tullis, T. E. (2007). Friction of rock at earthquake slip rates. In G. Schubert (Ed.), *Treatise on geophysics, volume 4: Earthquake seismology* (pp. 131–152). Amsterdam: Elsevier. <https://doi.org/10.1016/B978-044452748-6.00064-X>
- Tullis, T. E., & Weeks, J. D. (1986). Constitutive behavior and stability of frictional sliding of granite. *Pure and Applied Geophysics*, 124(3), 383–414. <https://doi.org/10.1007/BF00877209>
- Uchide, T., & Imanishi, K. (2016). Small earthquakes deviate from the omega-square model as revealed by multiple spectral ratio analysis. *Bulletin of the Seismological Society of America*, 106(3), 1357–1363. <https://doi.org/10.1785/0120150322>
- Uchide, T., Shearer, P. M., & Imanishi, K. (2014). Stress drop variations among small earthquakes before the 2011 Tohoku-oki, Japan, earthquake and implications for the main shock. *Journal of Geophysical Research: Solid Earth*, 119, 7164–7174. <https://doi.org/10.1002/2014JB010943>
- Wald, D. J., & Heaton, T. H. (1994). Spatial and temporal distribution of slip for the 1992 Landers, California, earthquake. *Bulletin of the Seismological Society of America*, 84(3), 668–691.
- Wang, Y., & Day, S. M. (2017). Seismic source spectral properties of crack-like and pulse-like modes of dynamic rupture. *Journal of Geophysical Research: Solid Earth*, 122(8), 6657–6684. <https://doi.org/10.1002/2017JB014454>